

Article

Testbed for Experimental Characterization of Indoor Visible Light Communication Channels

Miqueas Fortes and Oswaldo González * 

Department of Industrial Engineering, Universidad de La Laguna, Av. Astrofísico Francisco Sánchez, s/n, 38203 La Laguna, Spain; mfortesg@ull.edu.es

* Correspondence: oghdez@ull.es

Abstract: In this paper, we describe an experimental testbed designed to evaluate indoor visible light communications (VLC) in realistic scenarios. The system is based on a mockup where the location and orientation of the optical receiver can be modified with precision for a static configuration of walls and ceiling lamp arrangements. The system utilizes a timing synchronization method, which is based on evaluating the training sequence periods used for channel response estimation, which enables robust frame synchronization. In addition, an adaptive rate orthogonal frequency-division multiplexing (OFDM) scheme is used to assess the VLC performance throughout the receiver plane emulating a real communication. The preliminary results obtained with this prototype, considering a multiple-input single-output (MISO) scenario, demonstrate that reflection on walls yields a significant increase in data rates, which can be additionally improved if appropriate orientation of the receiver is implemented. However, vertical orientation upward of the optical receiver still constitutes a simple solution but efficient enough. Moreover, a good agreement between simulation and experimental results is observed, which confirms the suitability of the mockup as an experimental testbed for practical evaluation of indoor VLC systems, where system performance for different lamp arrangements and receiver designs, including multi-user communications, can be studied.

Keywords: Visible Light Communication (VLC); indoor channel characterization; Multiple-Input Single-Output (MISO) communication



Citation: Fortes, M.; González, O. Testbed for Experimental Characterization of Indoor Visible Light Communication Channels. *Electronics* **2021**, *10*, 1365. <https://doi.org/10.3390/electronics10111365>

Academic Editors: Jose A. Rabadan, Victor Guerra, Julio Rufo and Imran Shafique Ansari

Received: 21 April 2021

Accepted: 4 June 2021

Published: 7 June 2021

Publisher's Note: MDPI stays neutral with regard to jurisdictional claims in published maps and institutional affiliations.



Copyright: © 2021 by the authors. Licensee MDPI, Basel, Switzerland. This article is an open access article distributed under the terms and conditions of the Creative Commons Attribution (CC BY) license (<https://creativecommons.org/licenses/by/4.0/>).

1. Introduction

The dramatic demand for ubiquitous wireless data transfer in recent years has led to a renewed interest for alternatives to swamped radio communications, making visible light communication (VLC) an excellent, sustainable and energy-efficient candidate [1]. This technology is based on the use of visible (white) light-emitting diode (WLED) lamps to simultaneously illuminate but also provide data communication. In spite of the inherent advantages of this kind of wireless optical communication (WOC), mainly the possibility of working with high power transmission (visible light radiation at illumination levels is little harmful to the human eye) in addition to the fact that these communications are confined to a very small area (therefore enabling multiple high data rate communication cells in reduced space which are usually known as attocells [2]), there still exist many problems to solve [3].

Impressive Gigabit-per-second data rates at visible wavelengths have been reported in controlled laboratory experiments with perfect alignment between receivers and emitters [4,5], although these situations are not easily applicable to commercial solutions. Therefore, in many recent theoretical and experimental studies, the achievable data rates are less optimistic [6–8]. Another important issue is the necessity of a direct line-of-sight (LOS) between the emitter lamp and the receiver for a feasible communication, which is not always possible in a real environment where receiver orientation and shadowing effects are decisive in communication quality [9,10].

Downlink multi-user communications in indoor environments is one of the main current topics of VLC [11,12]. There exist many works oriented to characterize this indoor visible optical channel [13–15]. However, many studies have focused on demonstrating modulation methods or configuration networks for VLC, usually applying simpler channel models to evaluate their proposals (e.g., just considering the LOS component of the arriving signal), leading to overestimating the achievable data rates. Other works that include experimental demonstrations of their previous theoretical analysis usually develop testbeds, which are little representative of real indoor environments. This provokes a great gap between theoretical estimations [16] and real environment tests [17].

This work aims to develop an experimental testbed to provide deeper insight on the effects of non-LOS components of the radiated light and imperfect alignment between emitter lamps and receiver in indoor multi-user visible light communications from an experimental (not theoretical) point of view. The rest of the paper is organized as follows: Section 2 describes the main characteristics of indoor VLC channels. In Section 3, the testbed designed for experimental evaluation of VLC systems is presented, describing its physical characteristics and the implemented communication scheme. Section 4 shows the simulation results performed so as to assess the suitability of the mockup to evaluate indoor VLC scenarios. Section 5 presents the experimental results obtained with the manufactured mockup and, finally, the main conclusions of this work are summarized in Section 6.

2. Indoor Visible Light Channel

Figure 1 shows an illustration of the indoor VLC environment, where each lamp is composed of several LED chips whose light radiation contributes in the total received power. The radiation pattern of a LED is usually modeled as generalized Lambertian of order n [18]:

$$R_E(\phi) = P_E \frac{n+1}{2\pi} \cos^n \phi, \quad -\frac{\pi}{2} \leq \phi \leq \frac{\pi}{2}, \quad (1)$$

where P_E is the total power emitted by the LED and $n = -\ln 2 / \ln(\cos \phi_{1/2})$, being $\phi_{1/2}$ the transmitter semiangle (at half power). The LOS contribution of this LED to the received power at detector is obtained as an integration over the wavelengths λ of the emitted visible light [13]:

$$P_R = R_E(\phi) \int_{\lambda} p'(\lambda) A_{\text{eff}}(\phi) d\lambda / d^2 = P_E \frac{n+1}{2\pi d^2} \cos^n \phi A_r \cos \phi \int_{\lambda} p'(\lambda) d\lambda. \quad (2)$$

In the above equation, ϕ is the outgoing angle of light from the emitter towards the receiver, $A_{\text{eff}} = A_r \cos \phi$ the *effective area* of the detector of physical area A_r with the observation angle ϕ being the incoming angle of the light with respect to the normal of the detector surface, d the distance between emitter and receiver, and $p'(\lambda) = p(\lambda) / P_E$ the normalized power spectral density (PSD) of the WLED [13]. In Equation (2), $\int_{\lambda} p'(\lambda) d\lambda = 1$, thus the LOS contribution does not depend on the specific shape of the spectral emission characteristic of the LED. However, it is relevant when reflections on surfaces are also considered as we will see below. Moreover, this LOS contribution only occurs if the LED is in the field of view (FOV) of the receiver, that is, $\phi \leq \text{FOV} \leq \pi/2$.

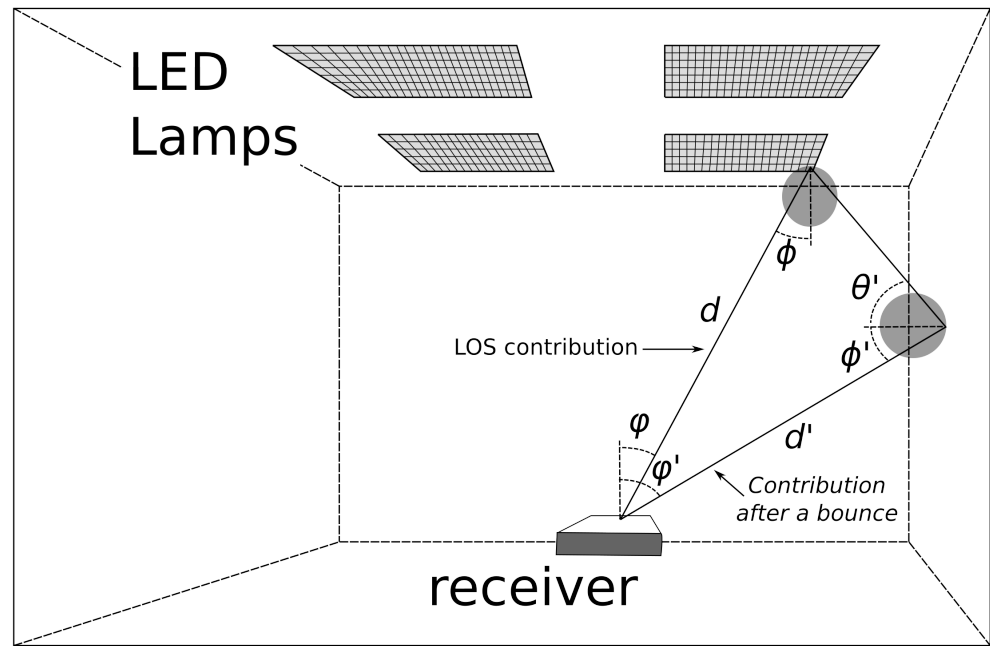


Figure 1. Illustration of the indoor VLC environment with LOS contribution of a single LED and its power contribution after off a wall.

In an indoor environment, there can be contributions to the total received power from emitted radiation that is reflected on walls or other surfaces inside the room. The reflection pattern of a surface at the wavelength λ can be approximated by the Phong’s model, which takes into account both diffuse and specular components of the light reflection [19]:

$$R_s(\phi', \theta', \lambda) = \rho(\lambda)P_I R'_s(\phi', \theta') \tag{3}$$

$$= \rho(\lambda)P_I \left[r_d \frac{1}{\pi} \cos \phi' + (1 - r_d) \frac{m + 1}{2\pi} \cos^m(\phi' - \theta') \right].$$

Here, r_d is the percentage of the received power that is reflected diffusely, $\rho(\lambda)$ the reflection coefficient of the surface, m the mode number of the specular component which defines its directivity, θ' the incoming angle of the incident ray, which impinges the surface with power P_I and ϕ' the outgoing angle of observation (see Figure 1).

To calculate the contribution after reflections, Monte Carlo based algorithms [20] randomly generate N rays according to the radiation pattern described in Equation (1) and determine the contribution of that ray after each collision and reflection off a surface. These algorithms have been demonstrated to be very accurate [21] and simultaneously with a much shorter simulation time than deterministic methods [22]. The contribution of a ray after its b th bounce to the total received power is [14]:

$$P_R^{(b)} = R'_s(\phi', \theta') A_{\text{eff}}(\phi') \frac{P_E}{N} \times \int_{\lambda} \rho_1(\lambda) \rho_2(\lambda) \dots \rho_k(\lambda) p'(\lambda) d\lambda / d'^2. \tag{4}$$

Here, $\rho_1(\lambda) \rho_2(\lambda) \dots \rho_k(\lambda)$ are the reflection coefficients of the corresponding surfaces against which it has collided, d' is the distance between the receiver and the last collision point (see Figure 1), $R'_s(\phi', \theta')$ is the normalized reflection pattern of this last surface (independent of $\rho(\lambda)$ and P_I) and $A_{\text{eff}}(\phi')$ the effective area at observation angle ϕ' . The remaining parameters keep the same meaning as in Equation (2).

Each lamp is composed of N_{LED} . Therefore, the total received power due to the l th WLED lamp can be calculated as the sum of the LOS component and contributions of the reflected light of rays generated from each of its LEDs:

$$h_l(t) = \mathcal{R} \sum_{k=0}^{K_{\Delta t}-1} p_k^{(l)} \delta(t - k\Delta t). \quad (5)$$

Here, \mathcal{R} is the detector *responsivity*, $\delta(t)$ is the Dirac's delta function and $p_k^{(l)}$ is the total power contribution (of all the N_{LED} LEDs composing l th lamp) received at k th time interval of the total of $K_{\Delta t}$ (of duration Δt) into which simulation time is discretized. From Equation (5) is inferred that the distribution of LEDs in the lamp affects the obtained impulse response. In this work, we have considered small square-shape lamps with uniform distribution of their LEDs, thus the combined effect of LEDs is practically identical to having a single LED source of total emitted power $P = N_{\text{LED}} \times P_E$, but any other distributions in larger lamps could be possible in practice.

The noise in a VLC link is mainly composed of shot noise due to the own transmitted signal and the ambient light if this reaches the interior of the room during daylight hours, plus a component of thermal noise [18]. Theoretically, for a well-designed receiver, the shot noise dominates and signal-to-noise ratios (SNR) above 60 dB can be achieved for room illumination standard levels above 400 lx [14,23]. However, experimental tests have usually demonstrated SNR up to ~ 30 dB due to thermal noise and design impairments [24,25], which limits the average channel capacity to 4–5 bit/s/Hz [26].

3. Experimental Testbed

Most of experimental demonstrations of proposed modulation and multiple access methods consider laboratory experiments under very controlled conditions. Misalignment or light reflection effects are out of the analysis, therefore leading to best-case studies. On the other hand, real-time systems are aimed to evaluate the possibilities of VLC at real distances but avoiding considering worst-case scenarios, such as bad alignment between emitting lamps and receiver [17,27,28]. In this work, we propose the design of a testbed which allows us to evaluate these effects usually overlooked from an experimental point of view. The testbed is a mockup where several lamps with different arrangements can be located and where the position and orientation of the receiver can be controlled. The reduction to a small scale implies that the VLC channel dispersion observed in a real room scenario no longer stands. However, as we will see in Section 4, these effects are little significant at practical data rates for VLC systems and they can be neglected. In addition, the emission power of WLEDs can be adjusted to obtain a similar scenario to that of a real room considering illumination and received power levels, so the testbed results can be extrapolated to real indoor VLC environments.

3.1. Mockup Description

Figure 2 shows the design of a 0.6 m \times 0.6 m \times 0.3 m (length \times width \times height) mockup by using AutoDesk[®] Fusion 360. In this first version, the ceiling was equipped with four WLED lamps as it can be observed in the general scheme and the zoom of the ceiling of the mockup design. However, the ceiling can be easily modified to have different lamp arrangements. Configuring receiver location and orientation is enabled by using precise servo and stepping motor systems managed by an Arduino microcontroller. In addition, the interior of walls is painted with white plastic paint to emulate the effect of light reflection. Most of plastic pieces of this mockup were manufactured using 3D printers. Walls are fabricated with methacrylate by using laser cutter, which was also used to cut the metal bars to support the structure. Nylon filament was used to manufacture the pieces holding the LED electronic boards so as to dissipate heat during operation.

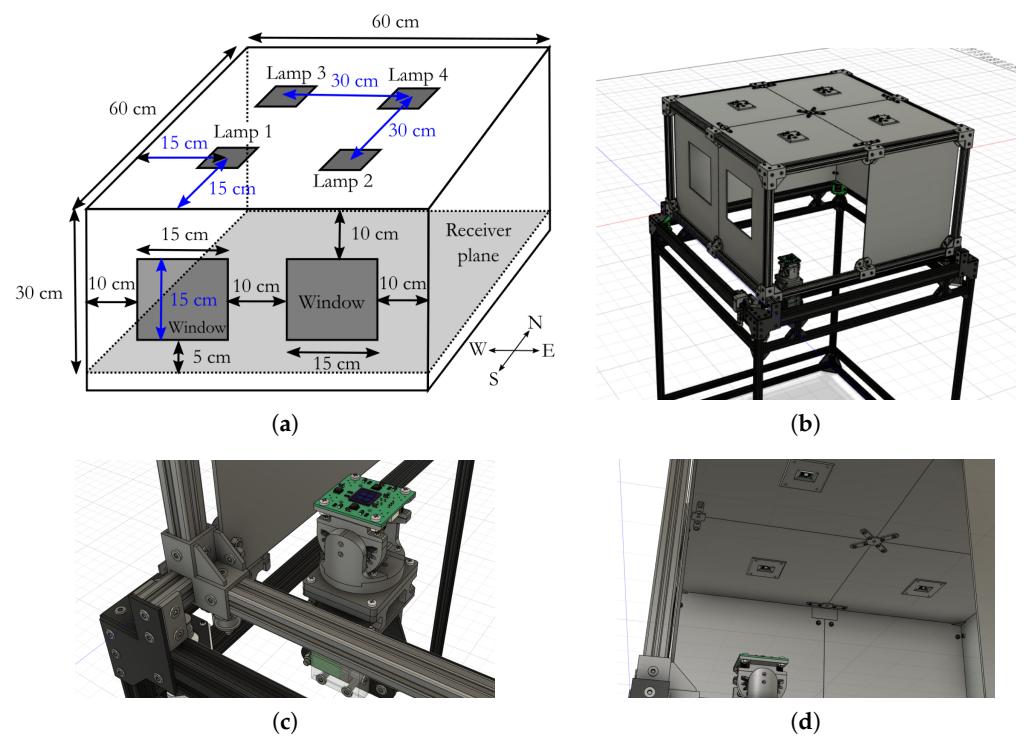


Figure 2. Mockup design: (a) Mockup scheme. (b) View of the mockup design. (c) Zoom of receiver. (d) Zoom of emitters at ceiling.

The optical receiver consists of a 2×2 matrix of photodetectors (Hamamatsu S5107 P-i-N photodiodes) with a total active area of 100 mm^2 connected to a transimpedance amplifier for each of the four channels. Emitters are based on standard commercial off-the-shelf (COTS) white LEDs which are fed by voltage-controlled current sources designed with operational amplifiers and power transistors. Figure 3 shows a 3D view of the electronic board designs of receiver and emitters by using KiCAD.

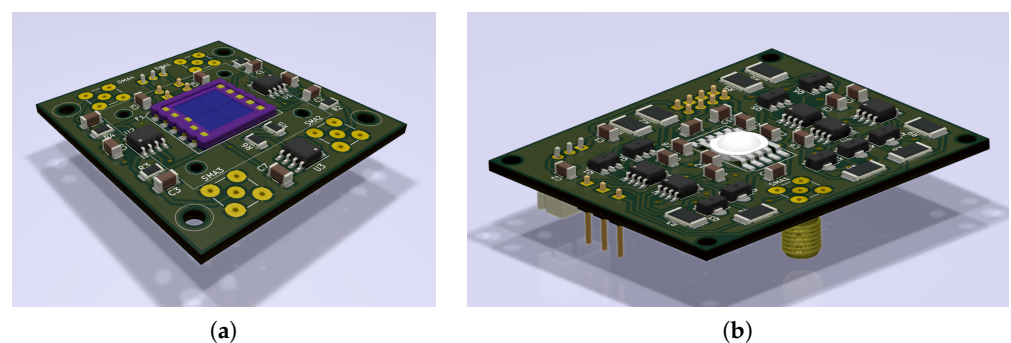


Figure 3. Electronic board designs: (a) Receiver board. (b) Emitter board.

3.2. Communication System

A typical orthogonal frequency-division multiplexing (OFDM) scheme for optical wireless communications was reported in [29], where the input data streams are encoded into quadrature amplitude modulated (QAM) orthogonal subcarriers (a total of $N_S - 1$) for parallel transmission. Note that the number of bits conveyed at a specific subcarrier depends on its SNR. The frequency separation between subcarriers is $\Delta f = B/N_S$, where B is the modulation bandwidth. The inclusion of a direct current (DC) bias ensures that the OFDM signal is all positive for intensity modulation of the LED. Moreover, to ensure a real-valued time domain signal Hermitian symmetry constraint must be met. This sequence is processed by an inverse fast Fourier transform (IFFT) block to obtain the $2N_S$ -sample

real-valued OFDM signal. Finally, prior to DC-biasing and low-pass filtering a N_E -sample cyclic extension is inserted to the signal at the output of the IFFT block to combat multipath induced intersymbol interference (ISI). At the receiver (Rx), the regenerated OFDM signal is down-sampled to obtain the $(2N_S + N_E)$ -sample sequence which, after removing the cyclic extension, is processed by a FFT block. Following this, just the $N_S - 1$ information-bearing symbols are considered throughout the last stages of channel equalization and, finally, QAM demodulation is performed to retrieve the transmitted data bit stream.

Due to the slowly time-varying VLC channel characteristics, the channel equalization can be implemented by transmitting training sequences to estimate the channel frequency response prior to the data transmission periods. By transmitting this training symbol an appropriate number N_{TS} of times it is possible to estimate the channel response at each specific n th sub-band as follows [29]:

$$\hat{H}_n = \frac{1}{N_{TS}X_n} \sum_{i=1}^{N_{TS}} Y_{n,i}, \quad (6)$$

where $Y_{n,i}$ is the received symbol at n th subcarrier during i th OFDM symbol of the training sequence of N_{TS} symbols, and X_n is the training symbol transmitted at that subcarrier, which is the same for all the OFDM symbols at a specific subcarrier. By adopting Saphiro-Rudin sequences [30] for training periods, which enables that certain gain can be applied to the sequence before transmitting due to their low peak-to-average ratio, N_{TS} of 20 would be enough to obtain an accurate estimate of H_n [29]. Therefore, N_{TS} is set to this value during experimental system evaluation.

Adaptive rate algorithms can be applied to enhance the system throughput by tailoring the bits conveyed by each subcarrier to its current available SNR. In this work, a simple and efficient bit-allocation algorithm described in [31] has been adopted, which only performs bit-loading while maintaining a constant transmit power for each subcarrier. Nevertheless, adopting more complex bit- and power-loading algorithms have not shown to offer any noticeable improvement in the throughput in real scenarios [32]. Moreover, the proposed algorithm in this work is concerned with fitting the average probability error to a target, thus enabling additional bit-allocation compared with simple schemes based on just keeping all the subcarriers working below that target bit error rate (BER).

Following channel estimation, the received symbols r_n are demodulated to recover the transmitted symbols. The SNR at the n th sub-band can be estimated by averaging over a series of received symbols at that subcarrier during subsequent OFDM symbols, which is given as:

$$\gamma_n = \frac{\sum_i |\hat{s}_{n,i}|^2}{\sum_i |\hat{s}_{n,i} - r_{n,i}|^2}, \quad (7)$$

where $\hat{s}_{n,i}$ are the estimated transmitted symbols. The previous sub-band SNR values γ_n are compared with switching levels obtained from BER vs. SNR plots to select the modulation mode (including 'no transmission', that is, $b_n = 0$), which ensures that the instantaneous BER always remains below the specified target P_e [31]. Moreover, the eligible b_n 's are constrained to the set $\mathbf{B} = \{0, 1, \dots, b_{\max}\}$. With the proposed scheme lower-bound performance is achieved where each subcarrier fulfills the maximum BER requirement separately. However, a more ambitious scheme would be to accomplish a target BER on average. Thus, once the bits supported by each subcarrier are initialized, the subcarriers with modulation modes that can be increased without exceeding the system target BER are selected. The selection order is based on increasing the modulation mode of subcarriers that offers a relatively lower increase in the average error probability [31]. This process is repeated until the desired target BER is reached (but not exceeded) and is also completed when all the subcarriers convey the maximum allowed number of bits b_{\max} .

In this work, we propose a timing synchronization scheme based on the method suggested by Park et al. [33]. According to [33], the timing sequence must have the following form:

$$P_{\text{Park}} = [\mathbf{a}_{L/4} \mathbf{b}_{L/4} \mathbf{a}_{L/4}^* \mathbf{b}_{L/4}^*], \quad (8)$$

where $\mathbf{a}_{L/4}$ represents a block of length $L/4$ samples generated by the IFFT (L -point) of a pseudo noise (PN) sequence, $\mathbf{b}_{L/4}$ is designed to be symmetric with $\mathbf{a}_{L/4}$, and $\mathbf{a}_{L/4}^*$ and $\mathbf{b}_{L/4}^*$ representing the complex conjugates of $\mathbf{a}_{L/4}$ and $\mathbf{b}_{L/4}$, respectively. This symbol pattern can be easily obtained by generating a real-valued PN sequence on the even frequencies, while zeros are used on the odd subcarriers. This yields an IFFT output whose pattern coincides with that of Equation (8).

We propose using the training periods to simultaneously perform timing synchronization and channel estimation [34]. However, obtaining Park's timing sequence would imply to disable odd frequencies, which collides with the second functionality of channel estimation, the latter requiring transmission of training symbols on all subcarrier frequencies. Fortunately, a single $2N_S$ -sample Shapiro-Rudin sequence is characterized by its second half being symmetric with its first half, thus presenting the form $[\mathbf{a}_{L/4} \mathbf{b}_{L/4}]$. Therefore, since this training sequence is real-valued, that is, $\mathbf{a}_{L/4}^* = \mathbf{a}_{L/4}$ and $\mathbf{b}_{L/4}^* = \mathbf{b}_{L/4}$, two of them can be combined and transmitted consecutively to obtain the pattern of Equation (8), now for $L = 4N_S$. Finally, as a cyclic prefix is placed before each OFDM symbol to combat ISI, N_E samples are inserted between each two consecutive OFDM symbols, so Park's timing metric has to be revised to adapt with this new scenario. Park's metric is given by:

$$M(d) = \frac{|P(d)|^2}{(R(d))^2}, \quad (9)$$

where $P(d)$ and $R(d)$ are now redefined as follows:

$$P(d) = r(d)^2 + \sum_{k=1}^{2N} r(d-k-N_E) \cdot r(d+k) \quad (10)$$

$$R(d) = \sum_{k=0}^{2N} |r(d+k)|^2. \quad (11)$$

Apart from the joint combination of timing and channel estimation, another inherent advantage of the proposed scheme is that the timing metric is based on $4N_S + 1$ instead of the $2N_S + 1$ samples as being evaluated by Park's method, thus improving its robustness. Additionally, Shapiro-Rudin sequences are invariant, thus leading to a predictable performance as compared with variable performance of Park's proposal based on PN sequences [34].

4. Simulation Results

In this section, several simulation results are presented to assess the suitability of the mockup as testbed to evaluate indoor VLC systems. Table 1 includes the main simulation parameters where a cubic room ($4.0 \text{ m} \times 4.0 \text{ m} \times 2.75 \text{ m}$) with four WLED array lamps is considered. For the reflection coefficient $\rho(\lambda)$ of the room surfaces, the experimentally measured spectral reflectances given in [13] are used. The room also contains two windows similarly as illustrated for the mockup in Figure 2a.

Table 1. Parameters of VLC Simulation Scenario.

Parameter	Value		
Room size (length × width × height):	4.00 m × 4.00 m × 2.75 m		
Number of LED arrays (lamps):	4 (2 × 2)		
Number of LEDs per array:	25 (5 × 5)		
Dimensions of each LED array:	0.1 m × 0.1 m		
Positions of LED arrays (central point) (x, y, z) [m]:	array 1: (1.00, 1.00, 2.75) array 2: (3.00, 1.00, 2.75) array 3: (1.00, 3.00, 2.75) array 4: (3.00, 3.00, 2.75)		
LED Lambertian order (n):	1		
Power of a single LED (P _E):	400 mW		
Total LED lamp power (P):	10 W		
Receiver plane height:	0.75 m		
Total detector physical area (A):	1.00 cm ²		
Surface materials parameters [13]:	$\overline{\rho(\lambda)}$	r_d	m
Ceiling:	0.35	1	-
Floor:	0.55	1	-
Walls (plaster):	0.69	1	-
Windows (glass):	0.04	0	280
Windows dimensions (width × height):	1.00 m × 1.00 m		

Figure 4 shows the simulated received power and illuminance at the receiver plane. The receiver has been considered pointing upward. First of all, we can observe that the minimum standard level of 400 lx at workplaces is fulfilled throughout the room. In addition, it can be seen how the LOS component contributes with more than 70% of the total received power in most of locations (approaching 80% at the center of the room) except for areas close to the walls where contribution of reflected light becomes more significant. Moreover, in areas near the windows (south face of the room), LOS component contribution grows again (with respect to those closer to other walls) due to the loss of light, which goes away through the windows.

Figure 5 shows the simulated impulse responses at three locations for the receiver: under lamp 1 close to windows, at the center of the room and under lamp 4 near a corner without windows. As we can see, LOS component dominates the impulses responses although the percentage of contribution due to first and second order reflection of emitted light are significant. It can also be observed in Figure 5c,d how the $k = 2$ reflection contribution is higher than that of $k = 1$ for the receiver positioned at room center. This is because the light emitted from LEDs, which comes back to the ceiling after the first reflection on walls makes the ceiling (for $k = 2$) a big emitting surface, this effect being more noticeable when receiver is located at central area of the room where first order reflection decreases due to the greater distance to the room walls. The delay spread D of the impulse's responses $h(t)$ throughout the room can be computed as [18]:

$$D = \left[\frac{\int_{-\infty}^{\infty} (t - \mu)^2 h^2(t) dt}{\int_{-\infty}^{\infty} h^2(t) dt} \right]^{1/2}, \quad (12)$$

where the mean delay μ is given by:

$$\mu = \frac{\int_{-\infty}^{\infty} t h^2(t) dt}{\int_{-\infty}^{\infty} h^2(t) dt}. \quad (13)$$

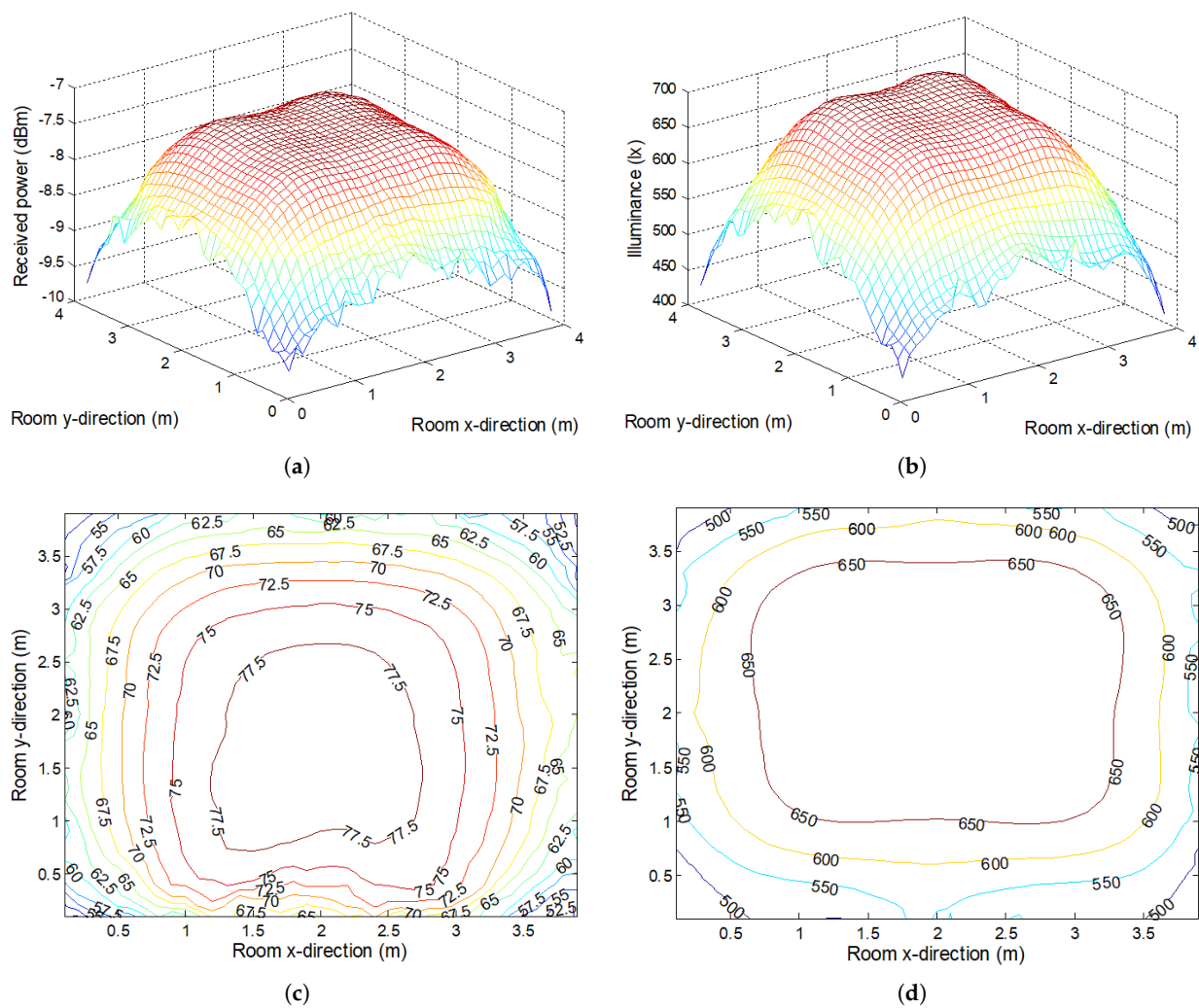


Figure 4. Received power and illuminance at receiver plane for room described in Table 1: (a) Power balance. (b) Illuminance. (c) Contour map of LOS component percentage in the total received power. (d) Contour map of illumination level.

Figure 6 depicts the mean delay and delay spread throughout the room at the receiver plane. It is seen as maximum delay spread hardly achieves 2.5 ns at room corners going below 1 ns for the central area of the room, leading to a coherence bandwidth of cents of megahertz. VLC systems based on affordable COTS devices are mainly limited to a few tens of MHz by LEDs and optical receiver bandwidths. Therefore, the temporal dispersion of the impulses responses due to the optical channel can be neglected for practical baud rates with communication bandwidths below 100 MHz.

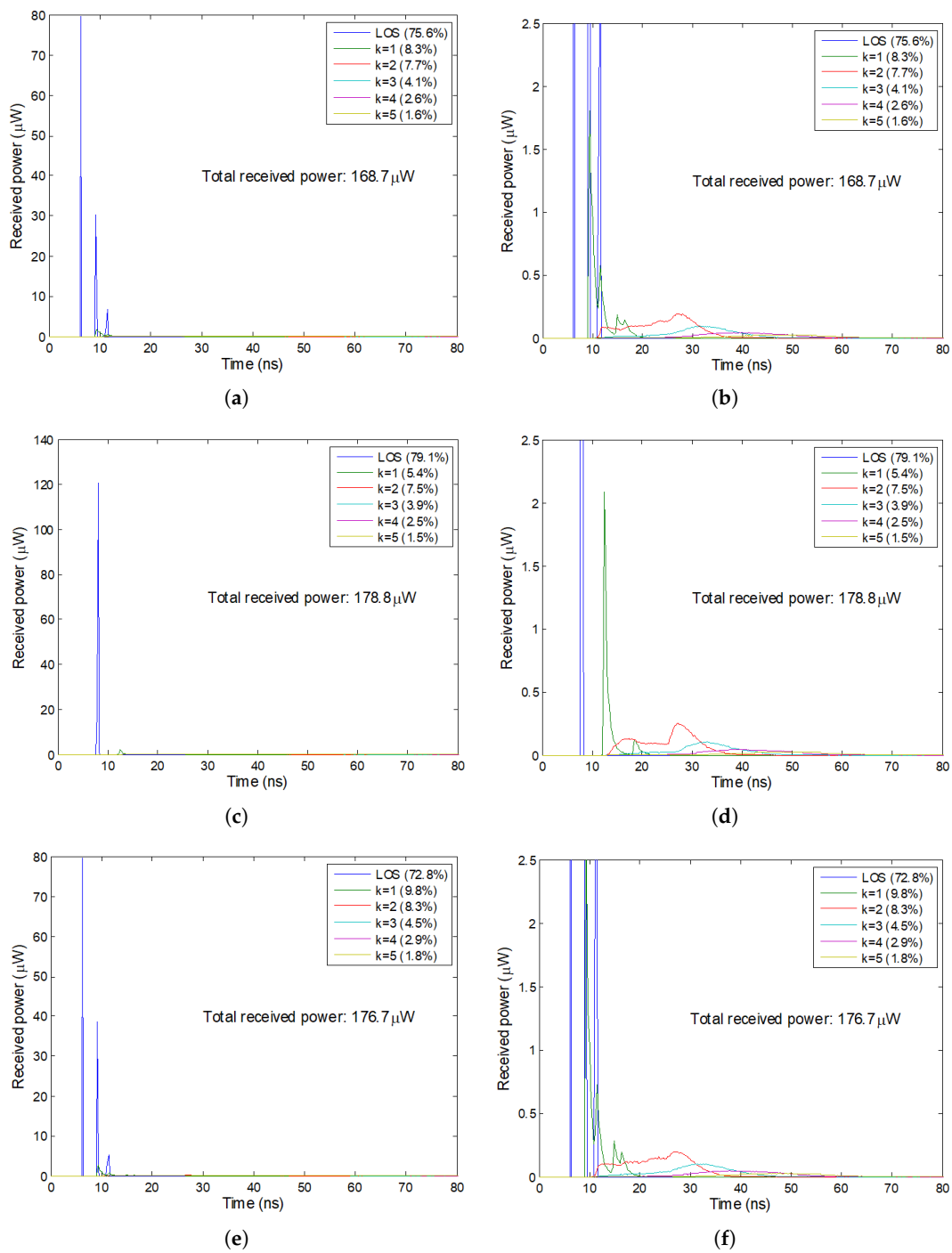


Figure 5. Simulated impulse responses at three locations: (a) Impulse response under lamp 1 (close to a window). (b) Zoom of impulse response under lamp 1. (c) Impulse response at the center of the room. (d) Zoom of impulse response at the center of the room. (e) Impulse response under lamp 4 (close to a corner). (f) Zoom of impulse response under lamp 4.

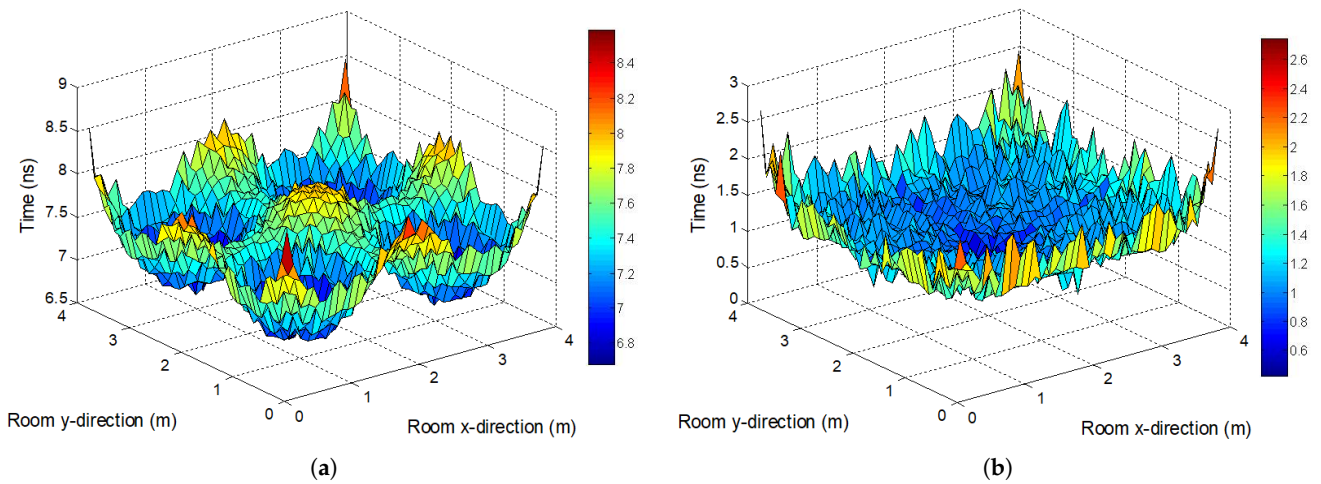


Figure 6. Simulated temporal dispersion of the impulse responses throughout the room: (a) Mean delay. (b) Delay spread.

When several lamps collaborate to send information to a certain user, the orientation of the detector can be optimized to maximize the total received power. Figure 7 represents an illustrative case when there are two lamps serving a certain user and it moves along the x-direction. Four configurations of receiver orientation are considered: ‘max’ indicates that the receiver is oriented to find the maximum received power as possible (this is the more complex case as the receiver has to look for all the possible orientations trying to maximize received power); ‘near’ stands for the case when the receiver is pointing to its nearest lamp; ‘vert’ symbolizes vertical orientation upward and ‘comb’ is referred to an orientation that is the combination of receiver position \vec{r}_{rec} with respect to each l th lamp weighted by the reciprocal of the square of its distance d_l to the lamp, that is, the receiver orientation is:

$$\vec{d}_{rec} = \sum_{l \in \mathcal{L}} (\vec{r}_l - \vec{r}_{rec}) / d_l^2, \tag{14}$$

where \mathcal{L} represents the set of lamps serving to this specific user and \vec{r}_l is the position of the l th lamp. The results of Figure 7 are presented for lamps with Lambertian order of $n = 1$ ($\phi_{1/2} = 60^\circ$) and $n = 2$ ($\phi_{1/2} = 45^\circ$), range of values where typical WLED radiation patterns are.

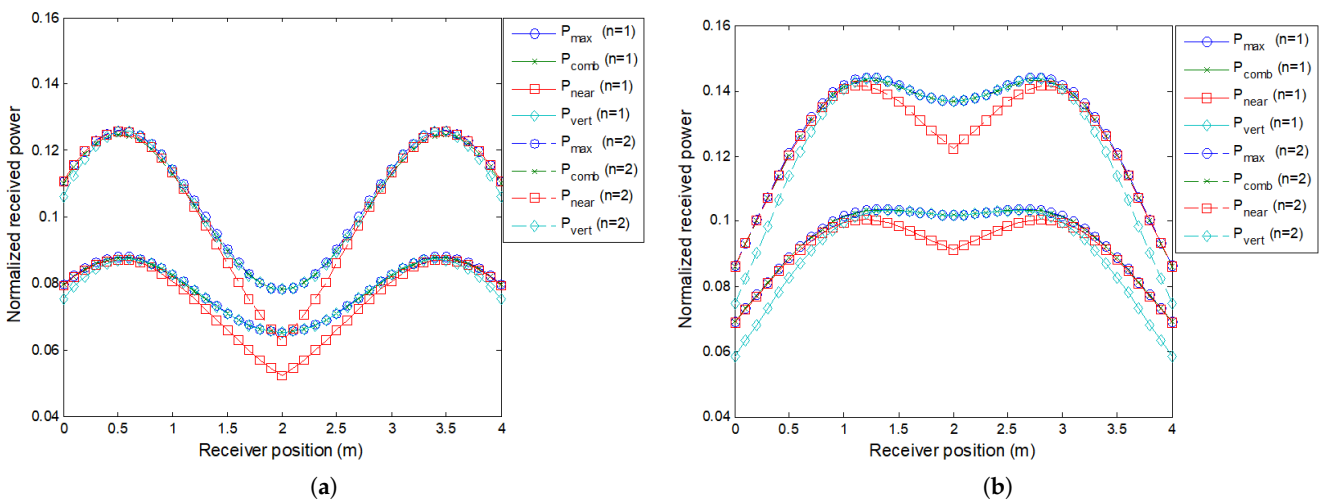


Figure 7. Received power from two lamps for different orientations of the receiver when it moves along the x-direction: (a) Results for a distance between lamps of 3 m. (b) Results for a distance between lamps of 2 m.

We can see how the method based on a weighted combination of the position of receiver with respect to emitting lamps almost approximates the impractical best case, the former requiring just the information about the location of the lamps which could be provided by a centralized positioning system. Pointing towards the nearest lamp also requires knowledge of lamps and receiver position but its behaviour is the worst. Just pointing upward constitutes a simple but almost quasi-optimum solution, specially if the distributions of lamps is good, which only requires gyroscope information of the hand-held device where the optical receiver is included. As we can see, for a distance of 3 m between both lamps, the received power fluctuates leading to an appreciable penalization at the central area. On the contrary, when this separation is reduced to 2 m, the received power is more uniform along x-axis with gradual decrease at the edge areas and vertical orientation works quite well. This is why we have defined a 2-m neighbor lamp separation arrangement for the simulated room (see Table 1), which serves as guide for our mockup design.

Figure 8 shows the power balance when the orientation method defined in Equation (14) is used so as to maximize the total received power from the four lamps. The figure also illustrates the elevation (angle from the vertical) and azimuth (angle from the x-axis in the XY plane) for the different locations of the receiver throughout the room. It is clear to see how the receiver is always oriented to a certain point in the center of the ceiling. Some increase in the received power with respect to force vertical orientation of the receiver is observed as well as a greater percentage of the LOS contribution at edge areas. This percentage is also more uniform and with a rectangular shape as reflection on walls becomes less significant due to the fact that the receiver is always pointing to a certain centroid of lamp positions, thus minimizing the observation of walls. Therefore, particular characteristics of each wall, for example, having windows or not, hardly affect the power balance.

A simulation for the mockup design illustrated in Figure 2 was conducted so as to compare the obtained results with those of the real indoor VLC environment previously described. In order to observe similar power levels, the power transmitted by each LED lamp was reduced by a factor of approximately $(L_{\text{mockup}}/L_{\text{room}})^2$, where $L_{\text{mockup/room}}$ refers to length of the mockup/room, specifically 0.25 W. Table 2 summarizes the simulation parameters for the mockup scenario. Mockup surfaces are characterized identically as described in Table 1, excepting floor that is considered with null reflection coefficient as there is no floor in the mockup design yielding that all the light reaching this surface vanishes.

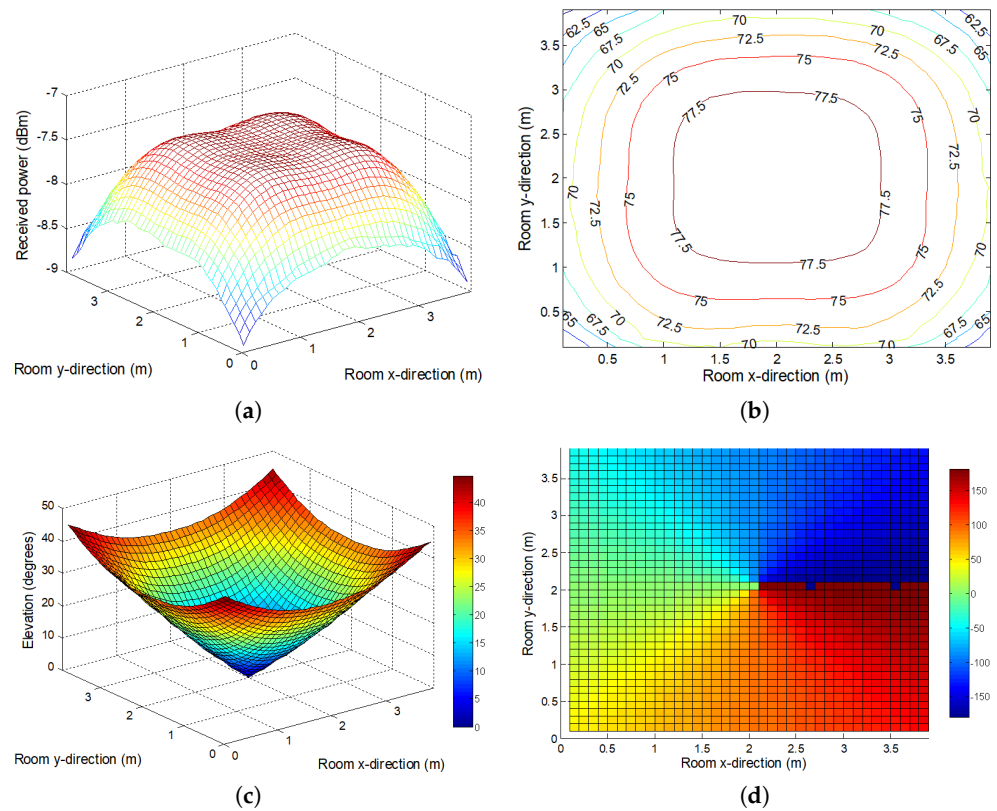


Figure 8. Received power throughout the room when the orientation method defined in Equation (14) is used: (a) Power balance. (b) Contour map of LOS component percentage in the total received power. (c) Elevation of the receiver as a function of its position. (d) Azimuth of the receiver as a function of its position.

Table 2. Parameters of Simulation for Mockup Scenario.

Parameter	Value
Room size (length × width × height):	60 cm × 60 cm × 30 cm
Number of LED arrays (lamps):	4 (2 × 2)
Number of LEDs per array:	9 (3 × 3)
Dimensions of each LED array:	0.1 m × 0.1 m
Positions of LED arrays (central point) (x, y, z) [cm]:	array 1: (15, 15, 30) array 2: (45, 15, 30) array 3: (15, 45, 30) array 4: (45, 45, 30)
LED Lambertian order (n):	1
Total LED lamp power (P):	250 mW
Receiver plane height:	0 cm
Total detector physical area (A):	1.00 cm ²
Windows dimensions (width × height):	15 cm × 15 cm

Figure 9 presents the results obtained for the mockup communication scenario. We can observe similar behavior of the power balance and the illuminance as compared with those results for the room shown in Figure 4. The greater percentage of LOS contribution to the total received power is due to the elimination of the floor as a reflecting surface. Figure 10 illustrates the impulses responses obtained for two positions of the receiver in the mockup: under lamp 1 close to a window (see Figure 2) and at the center of the receiver plane. Although with shorter times due to the smaller dimensions of the mockup, we can observe very similar impulses responses to those obtained for the room scenario as

presented in Figure 5, just appreciating the slightly greater percentage of LOS contribution, which is a consequence that there is no floor in the mockup and a lot of light is lost without ever being reflected. Therefore, we can conclude that the designed mockup constitutes a good frame for the experimental evaluation of indoor VLC systems.

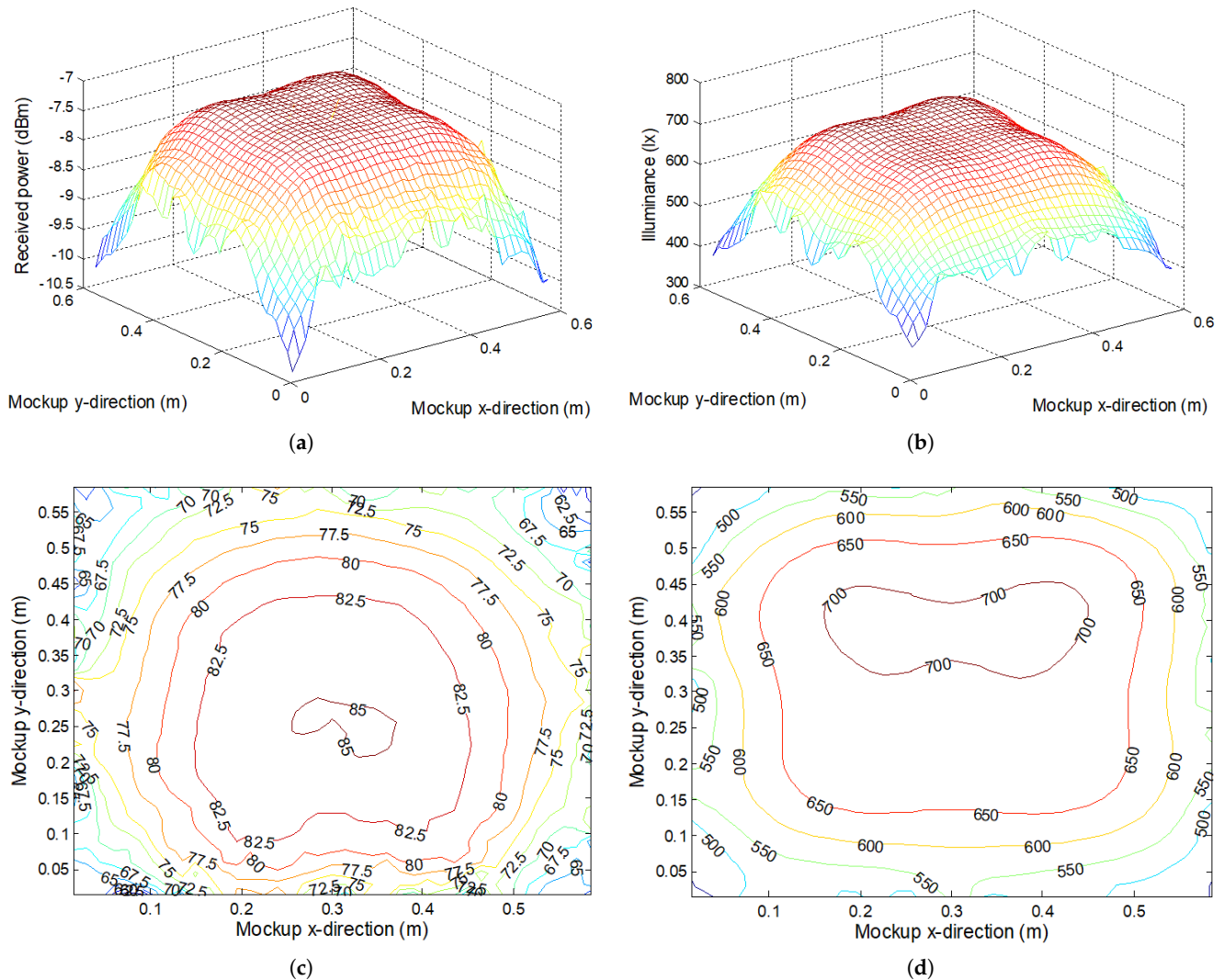


Figure 9. Received power and illuminance at receiver plane for mockup illustrated in Figure 2: (a) Power balance. (b) Illuminance. (c) Contour map of LOS component percentage in the total received power. (d) Contour map of illumination level.

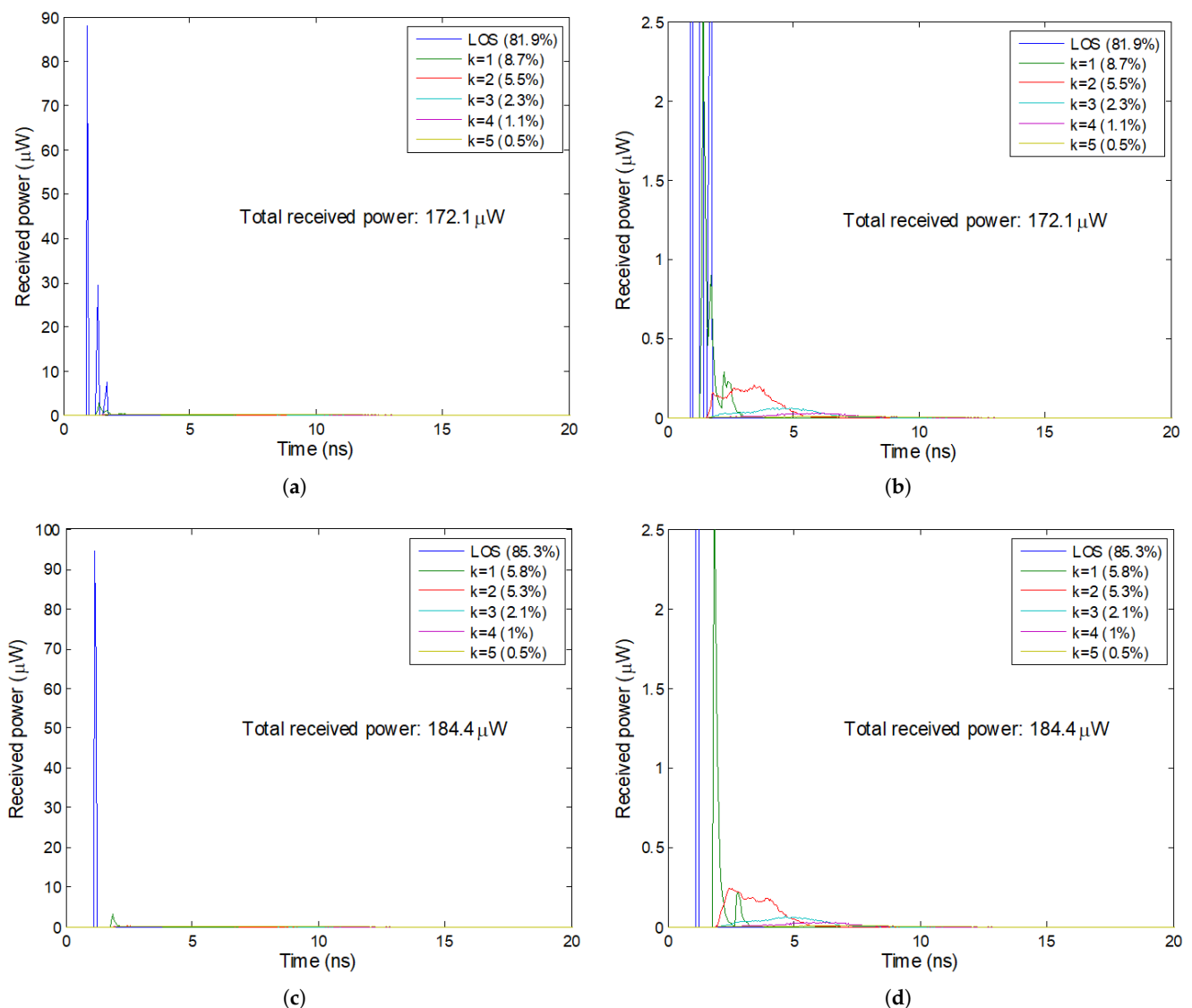


Figure 10. Simulated impulse responses at two locations of the mockup: (a) Impulse response under lamp 1 (close to a window). (b) Zoom of impulse response under lamp 1. (c) Impulse response at the center of the mockup. (d) Zoom of impulse response at the center of the mockup.

Once we know the power balance in the mockup, we can estimate the approximate data rate, which could be achieved throughout the receiver plane. Figure 11 shows the estimated throughput in bits per symbol (BPS) when adaptive OFDM is used as communication scheme (see Section 3.2). We have considered a fourth-order low-pass channel response with cut-off frequency at 65% of the communication bandwidth (which roughly fits typical VLC channel responses of experimental studies [24,25,32]) and a maximum SNR of 25 dB (at low frequencies) for the location at the center of the mockup receiver plane. Maximum SNR at other locations in the mockup are calculated based on the simulated received power at that location with respect to this reference level at the receiver plane center. For a target BER of 3.8×10^{-3} , two situations are evaluated: receiver pointing upward and receiver oriented as defined by Equation (14) to maximize received power. We can see how, in the second case, a more uniform throughput with higher values at edge areas is observed but still vertical orientation constitutes a simple and effective solution as previously mentioned.

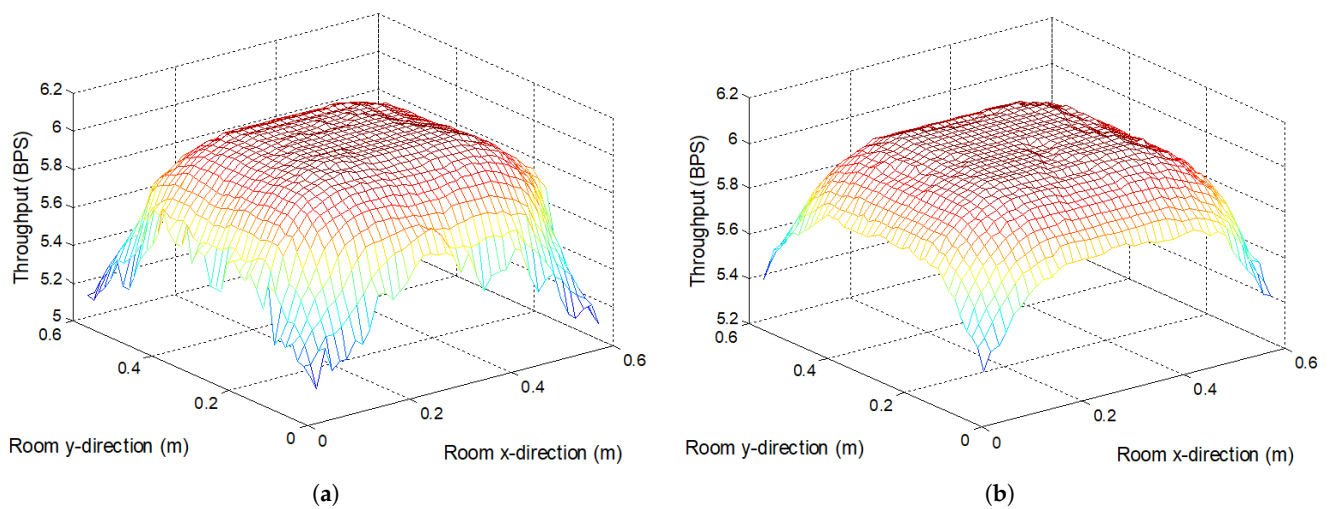


Figure 11. Simulated throughput in bits per symbol (BPS) at the receiver plane of the mockup by using the adaptive OFDM algorithm described in Section 3.2 (with $P_e = 3.8 \times 10^{-3}$) for two situations: (a) Receiver pointing upward ($th_{\max} = 6.1$ BPS, $th_{\text{mean}} = 5.8$ BPS, $th_{\min} = 5.1$ BPS). (b) Receiver oriented as defined by Equation (14) ($th_{\max} = 6.1$ BPS, $th_{\text{mean}} = 5.9$ BPS, $th_{\min} = 5.3$ BPS).

5. Experimental Results

Figure 12 illustrates different views of the mockup manufactured to experimentally evaluate VLC systems. In the general view of the testbed shown in Figure 12a, we can see the instruments controlled by a laptop: two arbitrary waveform generators Tektronix AFG31152 which are used to send the OFDM signals towards the four lamps and an oscilloscope Agilent MSO-X3052A which acquires the signal detected at optical receiver. Several tests have been developed to assess the suitability of this design. In this preliminary testbed evaluation, just one of the four channels of the 2×2 array of photodiodes Hamamatsu S5107 (the physical area of each photodetecting element is 0.25 cm^2) is acquired, configuring a multiple-input single-output (MISO) system. Use of the four channels, which are already operational, will be required in our future work which will be focused on studying MIMO schemes. The emitters are four standard red-green-blue (RGB) COTS LEDs not optimized for communication, thus the transmission bandwidth was established to 10 MHz. We consider that extensive commercial deployment of VLC systems will be carry out on standard LED luminaries, where transmission bandwidths will be limited to tens of MHz, therefore our design is in accordance with practical implementations similarly to other experimental studies [8,17,32].

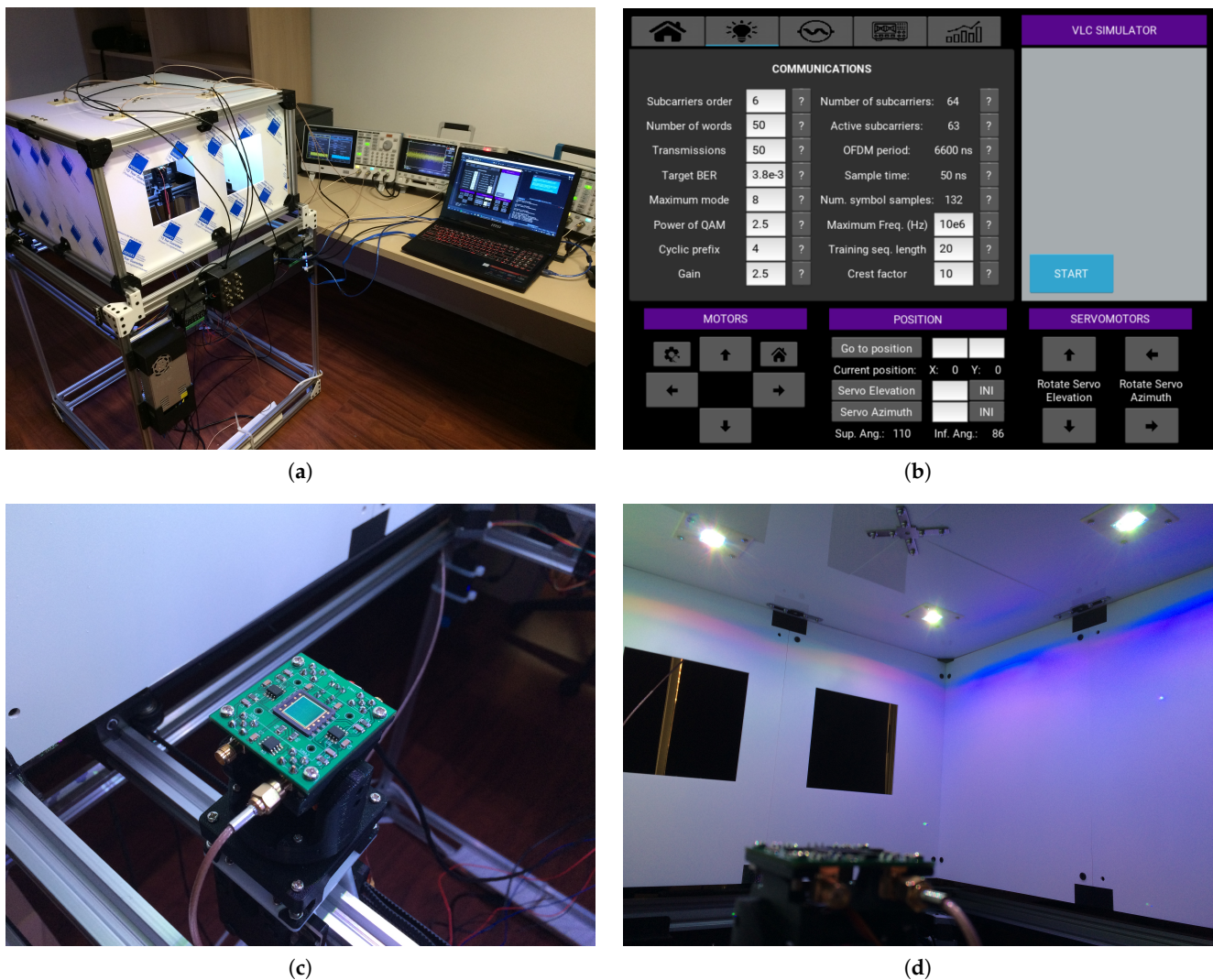


Figure 12. Views of the manufactured mockup: (a) General view of the experimental testbed. (b) Graphical user interface developed in Python. (c) Zoom of optical receiver. (d) Zoom of emitters at ceiling.

Table 3 presents the parameters set for the adaptive OFDM communication system during experiments as described in Section 3.2. Figure 13 shows some interesting results obtained when the receiver is located at the center of the mockup floor and the four lamps are transmitting the same information. Operating under the forward error correction (FEC) 7% BER limit of 3.8×10^{-3} , the achieved throughput was 4.8 BPS (45.4 Mbps for the transmission bandwidth of $B_T = 10$ MHz) with a measured BER of 1.5×10^{-3} . The achieved throughput is significantly inferior to the estimation depicted in Figure 11 for an ideal theoretical VLC channel, where many practical impairments are not modeled, for example, imperfect channel estimation, slight timing synchronization, sampling and acquisition errors, non-linear effects and clipping, and so forth at electronic devices. This reinforces the idea that experimental evaluation is crucial for a better characterization of VLC systems. Despite all the practical impairments, we can see how the measured BER is below the target, which demonstrates that the communication algorithm perfectly adapts to the actual channel situation during transmission. Moreover, with this testbed we are not interested in obtaining optimal data rates but evaluating throughput variations when the receiver situation inside the room changes.

Table 3. Parameters for Adaptive OFDM System.

Parameter	Value
Total number of subcarriers (N_S):	64
Number of information subcarriers (N_{SI}):	63
Maximum number of bits per subcarrier (b_{max}):	8 (256-QAM)
Target bit error rate (P_e):	3.8×10^{-3}
Modulation bandwidth (B_T):	10 MHz
Cyclic prefix extension (N_E):	4
OFDM symbol period (T_S):	6.6 μ s
Number of training sequences (N_{TS}):	20
Number of random-data symbols ($N_{symbols}$):	2500

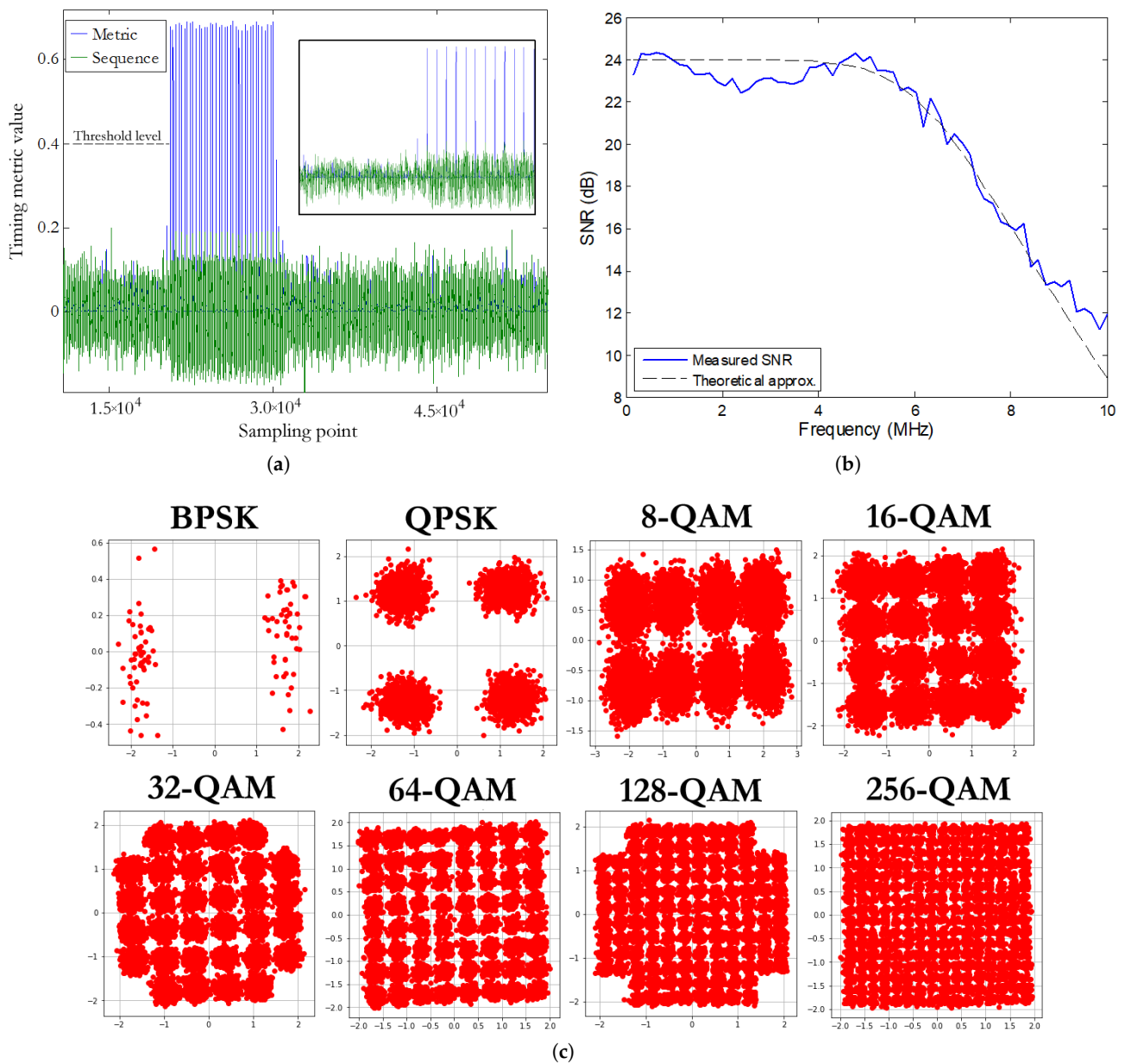


Figure 13. Experimental results obtained at the center of the mockup receiver plane when the four lamps transmit the same information: (a) Timing metric during a transmission. (b) Average of measured SNR. (c) Symbol constellations at receiver.

Figure 13a illustrates the timing metric during the evaluation of a received OFDM signal. The inset shows a transition between a random-data transmission and the start of a new training period. The narrow impulses shown in blue indicates the start of a new frame composed of $N_{TS} = 20$ training sequences and $N_{symbols} \gg N_{TS}$ OFDM sequences conveying the random data, which will be used for synchronization at the receiver end. The Shapiro-Rudin training sequences can be easily identified in the figure due to its characteristic shape. All the other impulses following the first impulse will be ignored by the synchronizing module. However, during the transmission of random-data OFDM symbols there are no impulses with sufficient height that will cross the dedicated threshold level. This timing method allows the receiver to synchronize with the incoming signal so as to proceed to perform channel estimation and data demodulation. There is no need for another different channel to carry out synchronization between emitted signals and receiver, thus a real optical communication is emulated. Additionally, Figure 13b presents the average of the measured SNR as compared with a theoretical fourth-order low-pass response. Finally, Figure 13c depicts the symbol constellations obtained at receiver end for this transmission.

Figure 14 shows the experimental throughput and SNR measured when just one lamp is used to transmit data. In all the experiments, the receiver was located defining a 7×7 matrix from an initial point $x = 7.5$ cm, $y = 7.5$ cm, with shift movements between neighboring positions of 7.5 cm in x- or y-direction. In addition, when not specified, the receiver was oriented vertically pointing upward during the test. Moreover, this one-lamp experiment was performed without walls, thus direct LOS links were evaluated. We can observe how the system throughput and SNR are degraded rapidly when the receiver moves beyond 30 cm (the half of the mockup width) from the lamp location (this can be seen more easily in the throughput map of Figure 17a). Therefore, the coverage radius, where the data rate is above the half of its maximum, is approximately the half of the communication room width. We can also see how there is a zone in the opposite area of the room to the lamp position where the communication was no possible (insufficient SNR was obtained and null data rate was observed). This prompts the idea that independent VLC links without almost interference between them could be established at opposite areas of the room but no more than two of these links could operate simultaneously because interference when receiver only moves in either x- or y-direction from the lamp is evident as the communication, although seriously degraded, is still possible. Therefore, a coordinated cooperative scheme between lamp transmissions would be required [12].

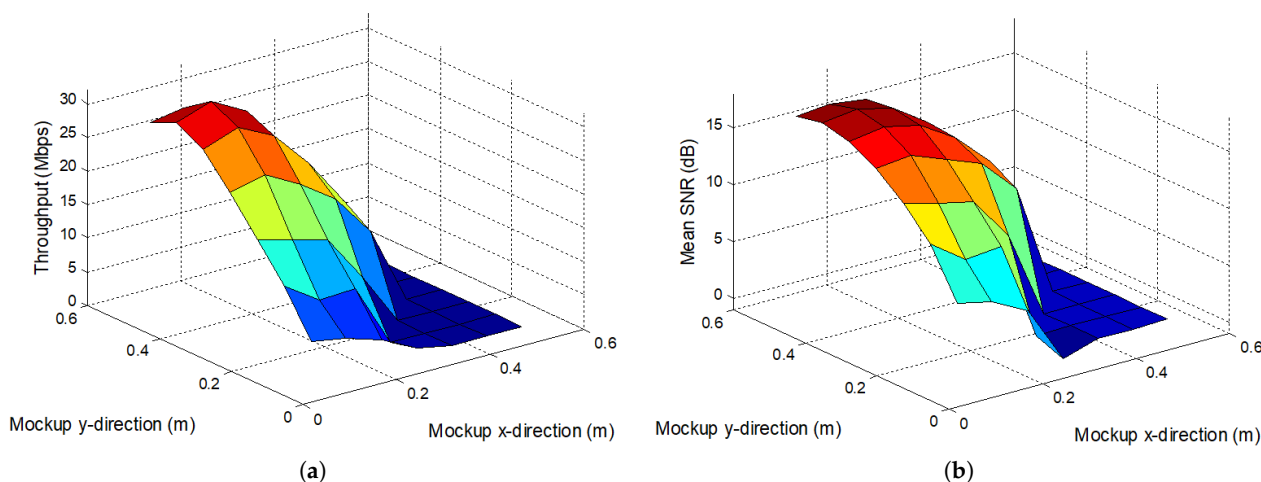


Figure 14. Experimental results with mockup when just one lamp is used to transmit data: (a) Measured throughput ($R_{\max} = 31.1$ Mbps, $R_{\text{mean}} = 17.3$ Mbps, $R_{\min} = 0.9$ Mbps for locations where communication was possible). (b) Measured mean SNR ($\overline{\text{SNR}}_{\max} = 17.3$ dB, $\overline{\text{SNR}}_{\text{mean}} = 13.5$ dB, $\overline{\text{SNR}}_{\min} = -0.9$ dB for locations where communication was possible).

When the four lamps are used to transmit the same information, the receiver can move freely throughout the room without experiencing a significant deterioration of the data rate as seen in the results presented in Figure 15. We can observe higher SNR values than those achieved for the one-lamp transmission (Figure 14) and thus the obtained data rates are greater too. The adaptive OFDM system was always able to work below the target BER of 3.8×10^{-3} . It is also noticeable how the measured illuminance throughout the mockup floor is above the recommendation for workplaces of at least 400 lx. More interestingly, these experimental results agree with the theoretical behavior predicted by simulations as depicted in Figures 9 and 11.

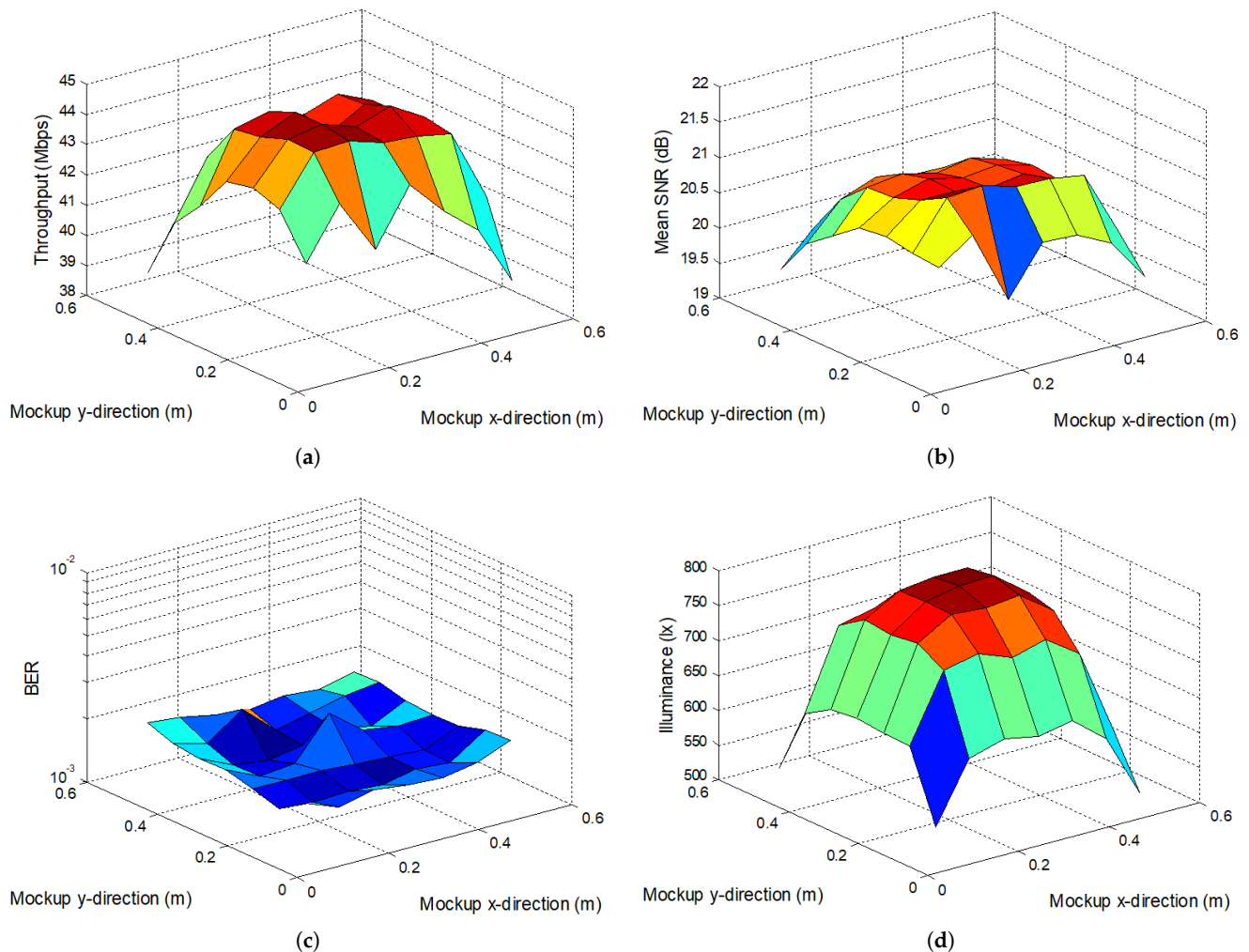


Figure 15. Experimental results for mockup without walls when the four lamps transmit the same data: (a) Measured throughput ($R_{\max} = 44.8$ Mbps, $R_{\text{mean}} = 42.8$ Mbps, $R_{\min} = 38.9$ Mbps). (b) Measured mean SNR ($\overline{\text{SNR}}_{\max} = 21.2$ dB, $\overline{\text{SNR}}_{\text{mean}} = 20.5$ dB, $\overline{\text{SNR}}_{\min} = 19.4$ dB). (c) Measured BER ($\text{BER}_{\max} = 2.4 \times 10^{-3}$, $\text{BER}_{\text{mean}} = 1.7 \times 10^{-3}$, $\text{BER}_{\min} = 1.4 \times 10^{-3}$). (d) Measured illuminance ($E_{\max} = 795$ lx, $E_{\text{mean}} = 681$ lx, $E_{\min} = 500$ lx).

Figure 16 compares the system performance for vertical pointing upward of the optical receiver and an orientation defined by its relative position with respect to all its serving lamps (in this case, the four lamps) calculated with Equation (14) when mockup walls are also added. Firstly, the inclusion of walls yields a significant increase in the obtained throughput and the measured mean SNR as compared with the results without walls presented in Figure 15, even at the center of the room, which demonstrates that the influence of light reflection cannot be ignored as it is usual in many studies where just LOS component is considered. We can see mean data rate improvements of about 5% at the central area of the room and of more than 10% at edge zones (outer rectangle of the matrix of receiver locations) while working below the target BER of 3.8×10^{-3} . In addition, an appropriate orientation of the optical receiver leads to an extra throughput enhancement of about 1% in average at edges zones but practically identical behavior at the central area of the room with a slightly more uniform distribution throughout the receiver plane. However, as it was also observed in simulation results, vertical orientation of the receiver still maintains a suitable throughput uniformity thanks to the contribution of reflected light, while being a simple solution because the receiver only requires a gyroscope (sensor usually incorporated in hand-held devices like smartphones) to correct its vertical orientation as compared with also requiring according to Equation (14) precise relative positioning information of all its serving lamps to be provided by a centralized system. Moreover, inaccuracies of this positioning information could lead to a worse performance than that obtained with the simpler solution of applying vertical orientation. In addition, there exist other practical impairments such as power intensity deviations among lamps that can affect more appreciably the overall system behavior.

To summarize, Figure 17 illustrates the throughput maps for the different configurations evaluated with the experimental testbed: vertical receiver orientation for one-lamp transmission, four-lamp transmission with and without walls, and four-lamp transmission with walls and receiver orientation given by Equation (14). It is clear that perfect map symmetry is not observed for the measured data rates which is due to practical differences among distinct lamps. We can also see for Figure 17c,d that at locations close to the windows (along x-axis, $y = 0$), the data rate experiences a slight decrease with respect to other equivalent positions where there are no windows, but not in such an evident way as it was observed in simulations. Therefore, we confirm that the experimental testbed provides realistic results affected by many practical impairments and slight variations among similar devices, thus offering certain new information for the evaluation of indoor VLC scenarios that is not possible or easy to model in studies based on simulations.

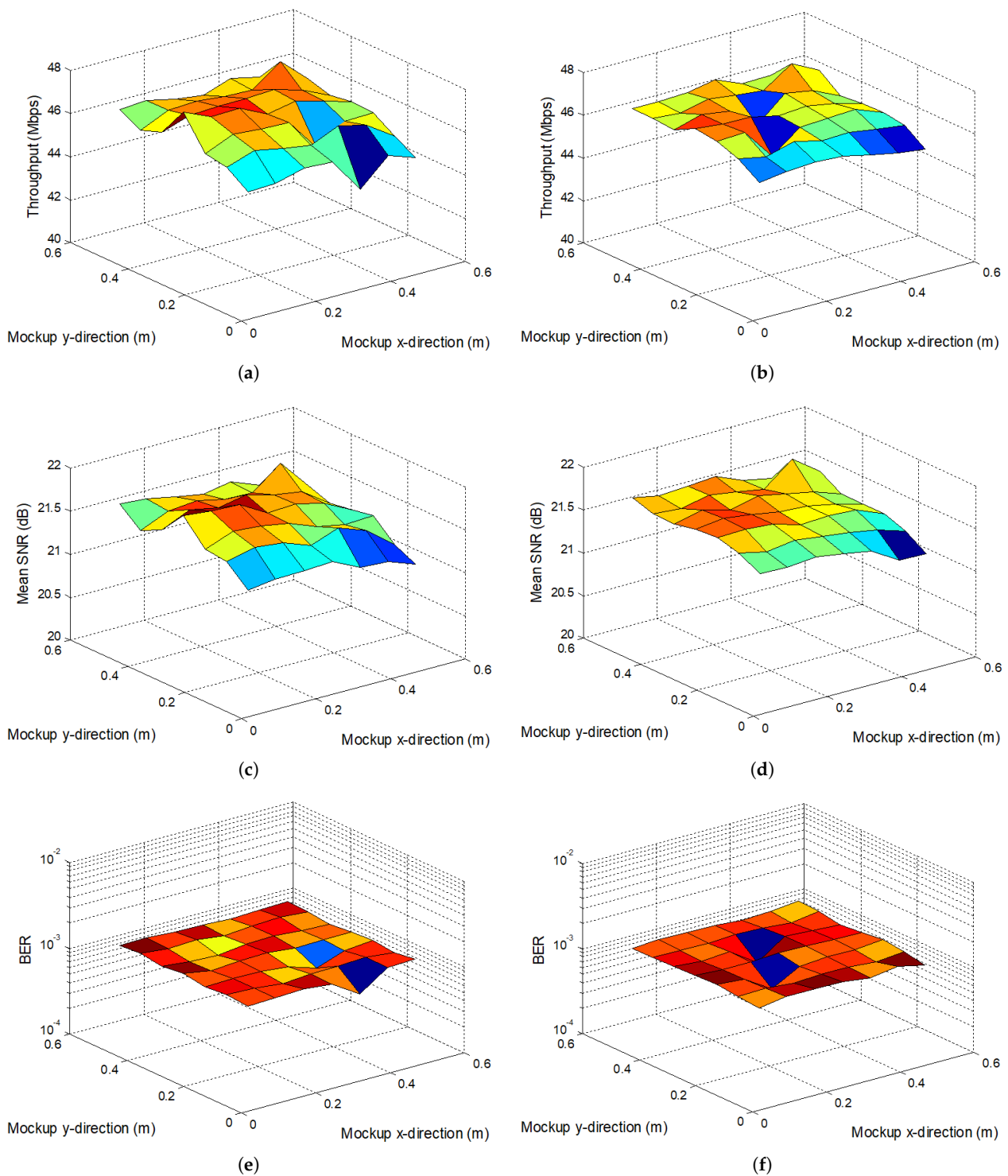


Figure 16. Experimental results for mockup with walls when the four lamps transmit the same data considering vertical orientation upward of the receiver and orientation given by Equation (14): (a) Measured throughput for vertical orientation ($R_{\max} = 47.5$ Mbps, $R_{\text{mean}} = 46.1$ Mbps, $R_{\min} = 43.9$ Mbps). (b) Measured throughput for receiver orientation given by Equation (14) ($R_{\max} = 47.2$ Mbps, $R_{\text{mean}} = 46.3$ Mbps, $R_{\min} = 45.2$ Mbps). (c) Measured mean SNR for vertical orientation ($\overline{\text{SNR}}_{\max} = 21.8$ dB, $\overline{\text{SNR}}_{\text{mean}} = 21.5$ dB, $\overline{\text{SNR}}_{\min} = 21.1$ dB). (d) Measured mean SNR for receiver orientation given by Equation (14) ($\overline{\text{SNR}}_{\max} = 21.8$ dB, $\overline{\text{SNR}}_{\text{mean}} = 21.5$ dB, $\overline{\text{SNR}}_{\min} = 21.2$ dB). (e) Measured BER for vertical orientation ($\text{BER}_{\max} = 1.2 \times 10^{-3}$, $\text{BER}_{\text{mean}} = 1.1 \times 10^{-3}$, $\text{BER}_{\min} = 0.7 \times 10^{-3}$). (f) BER for receiver orientation given by Equation (14) ($\text{BER}_{\max} = 1.2 \times 10^{-3}$, $\text{BER}_{\text{mean}} = 1.1 \times 10^{-3}$, $\text{BER}_{\min} = 0.7 \times 10^{-3}$).

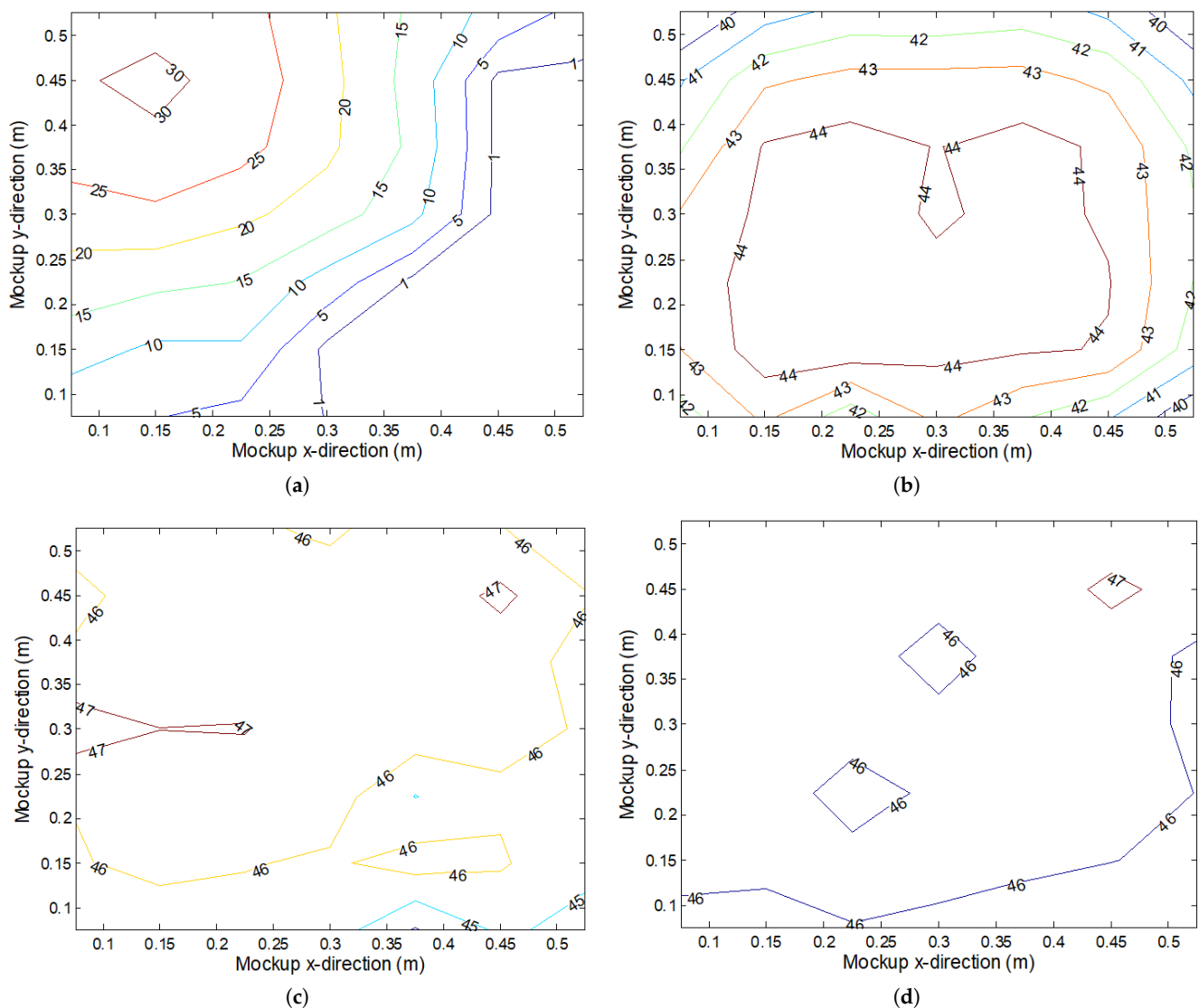


Figure 17. Summary of throughput maps for different configurations (if not specified, the receiver points vertically upward): (a) One-lamp transmission. (b) Four-lamp transmission without walls. (c) Four-lamp transmission with walls. (d) Four-lamp transmission with walls and receiver oriented as defined by Equation (14).

6. Conclusions

We have designed and manufactured a testbed for the experimental evaluation of indoor VLC schemes. In the developed mockup, the receiver position and orientation can be dynamically established with high precision for a static configuration of walls and arrangement of LED lamps on the ceiling. Adaptive rate OFDM with timing synchronization and channel equalization is implemented to evaluate the system performance as a function of the position and orientation of the optical receiver. Several simulation studies have been conducted so as to demonstrate the suitability of this small-scale prototype to be representative of real VLC scenarios. Preliminary experiments have been focused on studying single-user MISO systems, where a good agreement with simulation results has been observed. The positive influence of the contribution of reflected light in the measured throughput has been assessed, proving that this contribution should not be neglected as it is usual in many theoretical VLC studies, where only the LOS contribution is considered. Certain performance enhancement has also been observed when the optical detector is properly oriented trying to maximize received power from its serving lamps. However, vertical orientation upward still presents a good trade-off between ease of implementation and achievable data rates with lower practical performance deterioration than predicted

by simulations. These behavior differences between experimental and simulated results confirm the difficulty of adequately modeling every practical issue, which makes us conclude the need for this kind of testbed for a more realistic characterization of indoor VLC scenarios, providing additional information to the theoretical studies. Future work will be aimed at evaluating multi-user MIMO VLC systems with imaging and non imaging angular diversity reception, applying space-division multiple access (SDMA) or non-orthogonal multiple access (NOMA) [35].

Author Contributions: Conceptualization, O.G.; methodology, M.F. and O.G.; software, M.F. and O.G.; validation, M.F. and O.G.; formal analysis, O.G.; investigation, M.F. and O.G.; resources, M.F. and O.G.; data curation, M.F.; writing—original draft preparation, M.F. and O.G.; writing—review and editing, O.G.; visualization, M.F. and O.G.; supervision, O.G.; project administration, O.G.; funding acquisition, O.G. All authors have read and agreed to the published version of the manuscript.

Funding: This research has been funded by Spanish Government (Ministerio de Ciencia, Innovación y Universidades) and the European Regional Development Fund (ERDF/FEDER) program under project TEC2017-84065-C3-2-R.

Conflicts of Interest: The authors declare no conflict of interest.

References

1. Kavehrad, M. Sustainable energy-efficient wireless applications using light. *IEEE Commun. Mag.* **2010**, *48*, 66–73. [CrossRef]
2. Chen, C.; Basnayaka, D.A.; Haas, H. Downlink performance of optical attocell networks. *J. Lightwave Technol.* **2016**, *34*, 137–156. [CrossRef]
3. Pathak, P.H.; Feng, X.; Hu, P.; Mohapatra, P. Visible light communication, networking, and sensing: A survey, potential and challenges. *IEEE Commun. Surv. Tutor.* **2015**, *17*, 2047–2077. [CrossRef]
4. Azhar, A.H.; Tran, T.-A.; O'Brien, D. A Gigabit/s indoor wireless transmission using MIMO-OFDM visible-light communications. *IEEE Photon. Technol. Lett.* **2013**, *25*, 171–174. [CrossRef]
5. Bian, R.; Tavakkolnia, I.; Haas, H. 15.73 Gb/s visible light communication with off-the-shelf LEDs. *J. Lightw. Technol.* **2019**, *37*, 2418–2424. [CrossRef]
6. González, O.; Guerra-Medina, M.F.; Martín, I.R.; Delgado, F.; Pérez-Jiménez, R. Adaptive WHTS-assisted SDMA-OFDM scheme for fair resource allocation in multi-user visible light communications. *J. Opt. Commun. Netw.* **2016**, *8*, 427–440. [CrossRef]
7. Adnan-Qidan, A.; Morales-Céspedes, M.; García Armada, A. Load balancing in hybrid VLC and RF networks based on blind interference alignment. *IEEE Access* **2020**, *8*, 72512–72527. [CrossRef]
8. Chen, C.; Yang, Y.; Deng, X.; Du, P.; Yang, H. Space division multiple access with distributed user grouping for multi-user MIMO-VLC systems. *IEEE Open J. Commun. Soc.* **2020**, *1*, 943–956. [CrossRef]
9. Eroğlu, Y.S.; Yapici, Y.; Güvenç, I. Impact of random receiver orientation on visible light communications channel. *IEEE Trans. Commun.* **2019**, *67*, 1313–1325. [CrossRef]
10. Morales-Céspedes, M.; Genovés Guzmán, B.; Gil Jiménez, V.P. Lights and shadows: A comprehensive survey on cooperative and precoding schemes to overcome LOS blockage and interference in indoor VLC. *Sensors* **2021**, *21*, 861.
11. Zhang, R.; Wang, J.; Wang, Z.; Xu, Z.; Zhao, C.; Hanzo, L. Visible light communications in heterogeneous networks: Paving the way for user-centric design. *IEEE Wirel. Commun.* **2016**, *22*, 8–16. [CrossRef]
12. Obeed, M.; Salhab, A.M.; Alouini, M.-S.; Zummo, S.A. On optimizing VLC networks for downlink multi-user transmission: A survey. *IEEE Commun. Surv. Tutor.* **2019**, *21*, 2947–2976. [CrossRef]
13. Lee, K.; Park, H.; Barry, J.R. Indoor channel characteristics for visible light communications. *IEEE Commun. Lett.* **2011**, *15*, 217–219. [CrossRef]
14. González, O.; Guerra Medina, M.F.; Martín, I.R. Multi-user visible light communications. In *Advances in Optical Communication*; Das, N., Ed.; IntechOpen: Rijeka, Croatia, 2014; pp. 35–63. Available online: <https://www.intechopen.com/books/advances-in-optical-communication/multi-user-visible-light-communications> (accessed on 6 June 2021).
15. Uysal, M.; Miramirghani, F.; Narmanlioglu, O.; Baykas, T.; Panayirci, E. IEEE 802.15.7r1 reference channel models for visible light communications. *IEEE Commun. Mag.* **2017**, *55*, 212–217. [CrossRef]
16. Hussein, A.T.; Alresheedi, M.T.; Elmighani, J.M.H. Fast and efficient adaptation techniques for visible light communication systems. *J. Opt. Commun. Netw.* **2016**, *8*, 382–397. [CrossRef]
17. Haas, H.; Yin, L.; Chen, C.; Videv, S.; Parol, D.; Poves, E.; Alshaer, H.; Islim, M.S. Introduction to indoor networking concepts and challenges in LiFi. *J. Opt. Commun. Netw.* **2020**, *12*, A190–A203. [CrossRef]
18. Kahn, J.M.; Barry, J.R. Wireless infrared communications. *Proc. IEEE* **1997**, *85*, 265–298. [CrossRef]
19. Lomba, C.R.; Valadas, R.T.; de Oliveira Duarte, A.M. Experimental characterisation and modelling of the reflection of infrared signals on indoor surfaces. *IEEE Proc. Optoelectron.* **1998**, *145*, 191–197. [CrossRef]

20. López-Hernández, F.J.; Pérez-Jiménez, R.; Santamaría, A. Monte Carlo calculation of impulse response on diffuse IR wireless indoor channels. *Electron. Lett.* **1998**, *34*, 1260–1262. [[CrossRef](#)]
21. González, O.; Rodríguez, S.; Pérez-Jiménez, R.; Mendoza, B.R.; Ayala, A. Error analysis of the simulated impulse response on indoor wireless optical channels using a Monte Carlo based ray-tracing algorithm. *IEEE Trans. Commun.* **2005**, *53*, 124–130. [[CrossRef](#)]
22. Barry, J.R.; Kahn, J.M.; Krause, W.J.; Lee, E.A.; Messerschmitt, D.G. Simulation of multipath impulse response for wireless optical channels. *IEEE J. Sel. Areas Commun.* **1993**, *11*, 367–379. [[CrossRef](#)]
23. Grubor, J.; Randel, S.; Langer, K.-D.; Walewskik, J.W. Broadband information broadcasting using LED-based interior lighting. *J. Lightwave Technol.* **2008**, *26*, 3883–3892. [[CrossRef](#)]
24. Khalid, A.M.; Cossu, G.; Corsini, R.; Choudhury, P.; Ciaramella, E. 1-Gb/s transmission over a phosphorescent white LED by using rate-adaptive discrete multitone modulation. *IEEE Photon. J.* **2012**, *4*, 1465–1473. [[CrossRef](#)]
25. Tsonev, D.; Hyunhae, C.; Rajbhandari, S.; McKendry, J.J.D.; Videv, S.; Gu, E.; Haji, M.; Watson, S.; Kelly, A.E.; Faulkner, G.; et al. A 3-Gb/s single-LED OFDM-based wireless VLC link using a Gallium Nitride μ LED. *IEEE Photon. Technol. Lett.* **2014**, *26*, 637–640. [[CrossRef](#)]
26. Ma, S.; Yang, R.; Li, H.; Dong, Z.-L.; Gu, H.; Li, S. Achievable rate with closed-form for SISO channel and broadcast channel in visible light communication networks. *J. Lightwave Technol.* **2017**, *35*, 2778–2787. [[CrossRef](#)]
27. Grobe, L.; Paraskevopoulos, A.; Hilt, J.; Schulz, D.; Lassak, F.; Hartlieb, F.; Kottke, C.; Jungnickel, V.; Langer, K.-D. High-speed visible light communication systems. *IEEE Commun. Mag.* **2013**, *51*, 60–66. [[CrossRef](#)]
28. Shao, S.; Khreishah, A.; Ayyash, M.; Rahaim, M.B.; Elgala, H.; Jungnickel, V.; Schulz, D.; Little, T.D.C.; Hilt, J.; Freund, R. Design and analysis of a visible-light-communication enhanced WiFi system. *J. Opt. Commun. Netw.* **2015**, *7*, 960–973. [[CrossRef](#)]
29. González, O.; Pérez-Jiménez, R.; Rodríguez, S.; Rabadán, J.; Ayala, A. OFDM over indoor wireless optical channel. *IEEE Proc. Optoelectron.* **2005**, *152*, 199–204. [[CrossRef](#)]
30. Boyd, S. Multitone signals with low crest factor. *IEEE Trans. Circuits Syst.* **1986**, *33*, 1018–1022. [[CrossRef](#)]
31. González, O.; Pérez-Jiménez, R.; Rodríguez, S.; Rabadán, J.; Ayala, A. Adaptive OFDM system for communications over the indoor wireless optical channel. *IEEE Proc. Optoelectron.* **2006**, *153*, 139–144. [[CrossRef](#)]
32. Bykhovsky, D.; Arnon, S. An experimental comparison of different bit-and-power-allocation algorithms for DCO-OFDM. *J. Lightw. Technol.* **2014**, *32*, 1559–1564. [[CrossRef](#)]
33. Park, B.; Cheon, H.; Kang, C.; Hong, D. A novel timing estimation method for OFDM systems. *IEEE Commun. Lett.* **2003**, *7*, 239–241. [[CrossRef](#)]
34. Guerra Medina, M.F.; González, O.; Martín, I.R.; Rodríguez, S. Timing synchronization for OFDM-based visible light communication system. In Proceedings of the IEEE Wireless Telecommunications Symposium, London, UK, 18–20 April 2016; pp. 1–4.
35. Liu, Y.; Qin, Z.; El-kashlan, M.; Ding, Z.; Nallanathan, A.; Hanzo, L. Nonorthogonal multiple access for 5G and beyond. *Proc. IEEE* **2017**, *105*, 2347–2381. [[CrossRef](#)]